RESEARCH ARTICLE

Compact wideband MIMO mobile-antenna system design using mode-based decoupling techniques

Longyue Qu [ID] | Haiyan Piao | Hyeongdong Kim

Electronics and Computer Engineering, Hanyang University, Seoul, Republic of Korea

Correspondence
Hyeongdong Kim, Electronics and Computer Engineering, Hanyang University, Seoul, Republic of Korea.
Email: hdkim@hanyang.ac.kr

Abstract

This work focuses on designing small mobile antennas and their multiple-input multiple-output (MIMO) applications. In this study, it was investigated that small mobile antennas can obtain high radiation performance only when a tight coupling with the ground plane is generated through ground-mode tuning (GMT) of the ground plane. Furthermore, a novel mode-based decoupling concept is presented for their MIMO applications, based on a four-port network and by considering the ground-mode effect. Consequently, the proposed mode-based decouplers can effectively sustain high radiation performance and improve the isolation while providing low correlation by generating diagonally directed radiation patterns. In the proposed MIMO system, both GMT structures and mode-based decouplers are implemented utilizing the metal rims around the ground plane, thereby occupying very compact clearance, and the measured MIMO antennas fully covered 0.69 to 1 GHz band with high isolation up to 20 dB and low envelope correlation coefficient (ECC) value below 0.5, sufficiently applicable in mobile devices.

KEYWORDS

ground-mode tuning, metal rim, MIMO, mobile antennas, mode-based decouplers

1 | INTRODUCTION

With the development of wireless communications, market demands for mobile devices are increasing. Meanwhile, with the popularization of Fourth Generation (4G) and development of the next generation communication (5G), wideband multiple-input multiple-output (MIMO) antennas[1] are needed to meet the increasing requirements. With device integration, however, the printed-circuit boards (PCBs) and antennas are continuously being miniaturized, leading to electrically small antennas.[2] It is a great challenge for small antennas to achieve wideband performance because of their inherent properties, for example, high quality-factor (Q). In short, mobile antenna design is facing great challenges due to the miniaturization.

The normally used techniques for creating wideband antennas fall into three classes: antenna-geometry optimization,[3,4] parasitic-element employment,[5] and feeding-technique adoption.[6] However, all these conventional methods occupy large volumes, which cannot support the continuous miniaturization. Unlike conventional antenna techniques, ground-radiation antennas (GradiANT)[7–9] and capacitive coupling elements (CCE)[10–12] as well as ground-mode tuning (GMT) techniques[13–15] have been studied, which focus on the coupling mechanisms between the antenna and the ground plane, providing a valuable perspective for small mobile-antenna designs. Unfortunately, GradiANT suffers from narrow bandwidth, especially at low frequency bands, CCE is primarily dependent on the matching circuits, and the large volume of GMT structures remains as its main drawback.

In MIMO applications, antenna decoupling is an important factor to ensure high isolation, high efficiency, and low correlation. The normally used techniques include orthogonal polarization,[16–18] decoupling networks,[19–21] and additional decoupling structures (decouplers).[9,22–24] In the first

method, high isolation and low correlation are achieved by sacrificing one of the antennas, since only one ground mode can support good antenna performance, especially at the lower frequency. In the second method, the neutralization lines can only be used in specified cases and has not been reported in the lower frequency band, while the matching networks will severely degrade the efficiency and reduce the bandwidth. In the third method, few studies have reported at the lower frequency.

Accordingly, antenna ultra-miniaturization technique and its decoupling method in MIMO applications, that are suitable for modern smartphones and capable of providing characteristics of high isolation, low correlation, as well as broad impedance bandwidth and high radiation efficiencies, are greatly desired, especially at the lower frequency. Therefore, the principal idea of this study is to provide a framework for designing miniaturized and high-performance MIMO antenna system for mobile applications in the lower frequency band. Accordingly, this article focuses on two aspects:

1. A wideband small mobile-antenna design by increasing the coupling between the antenna and the ground plane to achieve high performance;
2. A novel decoupling concept for MIMO antennas to achieve simultaneously high isolation, low correlation, and wideband performance.

It is demonstrated that a tight coupling with the ground modes can guarantee the high performance of small antennas, which requires GMT such that the ground mode resonance is equal to the antenna operating frequency. Accordingly, two small slot antennas operating below 1 GHz are designed by GMT to the dominant mode of the ground plane using the top and the bottom metal rims, respectively. To introduce an effective and efficient decoupling technique to the MIMO antennas, a novel mode-based decoupling method using additional decouplers is investigated in a four-port network by considering the ground-mode effect. The decouplers are tightly coupled to the antenna elements for effective decoupling, while being loosely coupled to the tuned ground mode to maintain the antenna performance. As a result, two mode-based decouplers, utilizing the right and left metal rims, are implemented in the proposed small MIMO antennas, providing high isolation and diagonally directed radiation patterns.

The article is organized as follows: The operation mechanism of the small mobile antennas and the mode-based decoupling concept are demonstrated in Section 2. In Section 3, a small antenna using GMT is designed first, and two mode-based decouplers are implemented to their MIMO applications. Finally, the measurement is conducted to verify the simulation analysis.

2 | THEORETICAL ANALYSIS OF SMALL ANTENNAS

Input impedance of a small antenna is an important parameter for analyzing its radiation performance, which can be derived based on the two-port network involving the reaction theorem.[25,26] Accordingly, the corresponding input impedance of the antenna can then be calculated by

$$Z_{in} = Z_{aa} - \frac{(Z_{ag})^2}{Z_{gg}} \tag{1}$$

where

$$Z_{ag} = -\frac{1}{I_{ai}I_{gi}} \iint \int (\boldsymbol{E}_a \cdot \boldsymbol{J}_g) d\tau \tag{2}$$

In Equation (1), Z_{aa} is the self-impedance of the small antenna, which is dominantly reactive and nonradiative. Z_{gg} is the self-impedance of the ground plane, dominantly contributing to the far-field radiation. Z_{ag} is the mutual impedance between the antenna and the ground plane, which is associated with their mutual coupling. In Equation (2), I_{ai} and I_{gi} are the input currents at the input terminal of the antenna and the ground plane, respectively. $\boldsymbol{E}_a$ is the electric field generated by the antenna, and $\boldsymbol{J}_g$ is the current distribution in the ground plane. For mobile devices, only the dominant mode of the ground plane is near resonance, while all other modes are far away from resonance, especially at frequency below 1 GHz.

From the above analysis, we can observe the following:

1. The antenna impedance, particularly the radiation resistance, is significantly influenced by coupling to the ground modes, that is, a small mobile antenna operates as a ground radiation antenna[12,13]; and
2. The radiation performance can be optimized when the ground mode resonance is equal to the antenna operating frequency.[12,13,26]

In MIMO applications, however, severe isolation and correlation issues are introduced when both antennas are utilizing the same dominant mode of the ground plane. Previous analysis of the decoupling mechanism of decouplers based on a three-port network[9,22] is insufficient to develop effective and efficient decouplers, which can maintain the antennas' high efficiency and wideband performance while improving their isolation simultaneously. As can be known, the ground mode has been proved to be an important element to guarantee high radiation performance, so the adopted decouplers cannot degrade the ground-mode property or decrease the mutual coupling between the antennas

and the ground mode. Herein, a novel decoupling technique utilizing mode-based decouplers is investigated by considering the ground-mode effect based on a four-port network.

We designate ports 1, 2, 3, and 4 to be antenna 1, antenna 2, ground mode, and decoupler, respectively. We assume two antennas are simultaneously coupling to the same ground mode (port 3) for radiation. The general idea of the proposed four-port network is similar to the three-port network, which is implemented by putting a reactive load with proper values on the terminal of the decoupler (port 4), so that no voltage appears across antenna 2 (port 2) when a current source is applied at antenna 1 (port 1); i.e., the mutual impedance $Z_{12} = 0$.

The original impedance matrix in the four-port network, which is represented by voltages and currents, is

$$\begin{bmatrix} V_1 \\ V_2 \\ V_3 \\ V_4 \end{bmatrix} = \begin{bmatrix} Z_{11} & Z_{12} & Z_{13} & Z_{14} \\ Z_{21} & Z_{22} & Z_{23} & Z_{24} \\ Z_{31} & Z_{32} & Z_{33} & Z_{34} \\ Z_{41} & Z_{42} & Z_{43} & Z_{44} \end{bmatrix} \begin{bmatrix} I_1 \\ I_2 \\ I_3 \\ I_4 \end{bmatrix}. \tag{3}$$

It transforms into a new three-port impedance matrix, when port 4 is terminated by a load Z_L, as

$$\begin{bmatrix} V_1 \\ V_2 \\ V_3 \end{bmatrix} = \begin{bmatrix} Z'_{11} & Z'_{12} & Z'_{13} \\ Z'_{21} & Z'_{22} & Z'_{23} \\ Z'_{31} & Z'_{32} & Z'_{33} \end{bmatrix} \begin{bmatrix} I_1 \\ I_2 \\ I_3 \end{bmatrix} \tag{4}$$

where the load can then be written as

$$Z_L = -\frac{V_4}{I_4}. \tag{5}$$

By substituting Equation (5) into Equation (3) and rearranging, the modified impedance parameters can be achieved as

$$Z'_{12} = Z_{12} - \frac{Z_{14}Z_{24}}{Z_{44} + Z_L} \tag{6}$$

$$Z'_{11} = Z_{11} - \frac{Z_{14}Z_{41}}{Z_{44} + Z_L} \tag{7}$$

$$Z'_{22} = Z_{22} - \frac{Z_{24}Z_{42}}{Z_{44} + Z_L} \tag{8}$$

$$Z'_{33} = Z_{33} - \frac{Z_{34}Z_{43}}{Z_{44} + Z_L} \tag{9}$$

$$Z'_{13} = Z_{13} - \frac{Z_{14}Z_{34}}{Z_{44} + Z_L} \tag{10}$$

$$Z'_{23} = Z_{23} - \frac{Z_{24}Z_{34}}{Z_{44} + Z_L}. \tag{11}$$

Important insights can be obtained from the above extracted formulas.

1. In Equation (6), the first term in the right-hand part (Z_{12}) is the original mutual impedance between the two antennas, which is determined by both direct coupling between antenna elements and the coupling through the shared ground plane, while the latter would be closely associated with parameters such as Z_{13}, Z_{23}, and Z_{33}.

   Furthermore, it is obvious that Z_{12} can be modified as Z'_{12} by loading the decoupler, and Z'_{12} can be 0 (perfect decoupling) by properly modifying the second term in the right-hand part, where Z_{14}, Z_{24}, Z_{44}, and Z_L are important tunable parameters for decoupling. To achieve perfect decoupling between two antenna elements ($Z'_{12} = 0$) at a certain frequency, the loaded impedance at the decoupler should satisfy the following equation

$$Z_L = \frac{Z_{14}Z_{24}}{Z_{12}} - Z_{44} \tag{12}$$

2. The antenna impedance in Equations (7) and (8) can be altered when Z_L is loaded to the decoupler, and this effect can be well adjusted by impedance matching.

3. In Equation (9), the ground-mode property can also be modified if the mutual coupling between the decoupler and the ground mode, that is, Z_{34}, is strong. The ground mode has typically been optimized using GMT, so additional modification is not desired. More importantly, the decouplers are usually small compared to the ground plane, which would introduce more reactive components and extra ohmic loss, so a higher-Q mode can be generated with radiation-efficiency reduction if a tight coupling is generated between the decoupler and the ground mode. Therefore, Z_{34} should be minimized.

4. Furthermore, it can be seen from Equations (10) and (11) that the decouplers also affect the mutual coupling between the antennas and the ground mode, where Z_{14}, Z_{24}, and Z_{34} are three parameters. This effect is neglected if Z_{34} is minimized.

In summary, an optimal decoupler should reduce the mutual coupling between antennas without degrading the ground-mode characteristic or decreasing the coupling between the antennas and the ground mode. Equivalently, Z'_{12} should be tuned to zero without affecting Z_{13}, Z_{23}, and Z_{33}. Accordingly, Z_{14}, Z_{24}, Z_{44}, and Z_L should be optimized to decouple the antennas, while Z_{34} should be minimized.

Therefore, a decoupler that tightly couples with the antennas while loosely coupling with the ground mode is desired. This is the key point of the proposed mode-based decoupling technique for small mobile MIMO antennas. This technique provides a unique but general perspective to the MIMO design by considering the ground-mode effect. Based on the above guidelines, the proposed MIMO antennas was constructed and simulated based on Finite Element Method (FEM) using High-Frequency Structure Simulator (HFSS).

3 | ANTENNA SYSTEM DESIGN

3.1 | Single antenna design

In mobile applications, the ground-mode resonance is normally higher than the operating frequency, especially at low frequencies. Based on the above analysis in small antennas in Section 2, high radiation performance of a small antenna can be obtained by proper antenna implementation and GMT of the dominant mode along the length of the ground plane (along z-axis) to ensure a tight coupling with the ground modes. Accordingly, a slot antenna at the end of the ground plane is implemented for ground-mode excitation, as depicted in Figure 1. Since the theory of characteristic modes has been well analyzed and utilized in antenna engineering,[27–29] it is no longer discussed here. Details of the proposed antenna are as follows.

The ground plane is etched in a 1-mm-thick FR4 substrate ($\varepsilon_r = 4.4$, tan $\delta = 0.02$). The metal rims surround the ground plane 2 mm away and are placed along the x-axis with 4 mm in height. Four slits separate the metal rims into four parts: top, bottom, right, and left. The top and bottom rims have horizontal and vertical lengths of 64 mm and 10 mm, respectively. The bottom rims are connected to the ground plane by an inductor pin L (8 nH) at the center of the
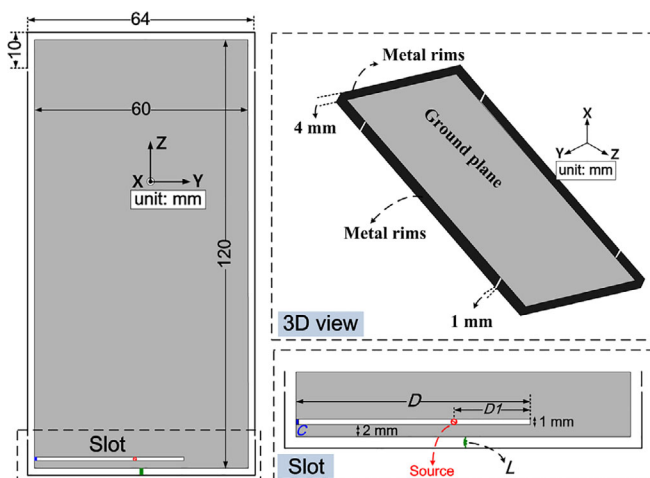
proposed GMT structures, so that the ground-mode resonance along the length of the ground plane can easily be tuned to the operating frequency by adjusting the values of L without changing the length of the rims. The slot is placed 2 mm away from the bottom edge of the ground plane, within a clearance of 1 mm $\times$ D mm (D = 42 mm). Meanwhile, the slot is fed by a voltage source at $D1$ = 12 mm, and lumped capacitor elements C (0.8 pF) are loaded to adjust the resonant frequency of the slot.
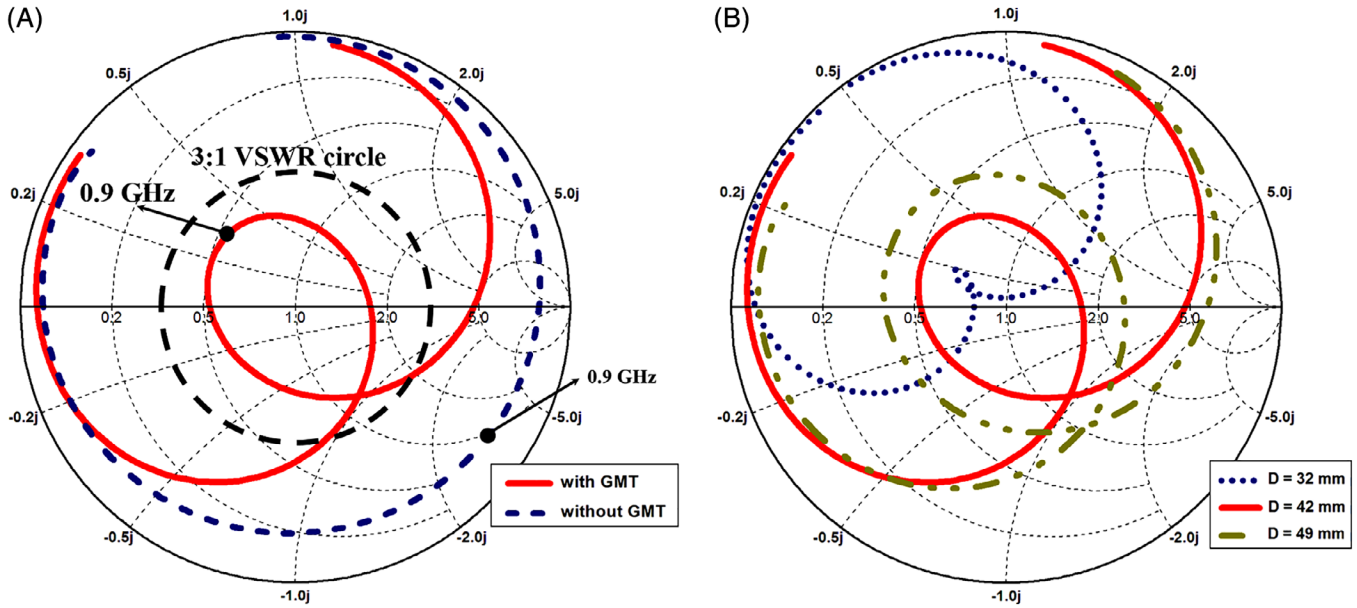
The proposed antenna design is an upgraded version of that in Reference [13], where both top and bottom metal rims were utilized for one antenna design, which suffers from large volume occupation, leaving little space to MIMO implementation. Furthermore, the proposed slot antenna is capacitor-loaded, so it is more desirable due to further miniaturization and easy integration. Though slot antennas operating lower than 1 GHz have been introduced in Reference [30,31], their clearance areas are much larger, which is not suitable for modern smartphone scenarios. For a better understanding of the operating mechanism of the proposed antenna design, the GMT technique and the excitation technique of the slot antenna are introduced in the following.

Figure 2A illustrates the input impedance loci of the slot antenna in a Smith chart with and without GMT (ie, with and without the inductor pin L). Significant differences can be observed in that the locus without GMT is dominantly reactive, whereas the locus with GMT presents dual resonance with a 3:1 voltage standing-wave ratio (VSWR) bandwidth from 0.75 to 1 GHz. Based on the analysis in Section 2, the ground-mode resonance is tuned approximately equal to the slot-antenna resonance (approximately 0.9 GHz) by the GMT structures, so the ground-mode resonance (the smaller locus at center) is excited due to a tight coupling, providing wide bandwidth.

Figure 2B depicts the effect of the slot length D in determining the mutual coupling with the ground mode. As D is decreased to 32 mm, the locus of the ground-mode resonance becomes smaller, indicating a reduction in the mutual coupling between the slot antenna and the tuned ground-mode resonance. The mutual coupling can be increased by increasing D to 49 mm, which can be seen from the enlarged impedance locus of the ground-mode resonance. It is evident that the length of the slot is a critical parameter to the mutual coupling, as indicated in Equation (2). Note that the data are obtained by also modifying the values of C and $D1$ to maintain the antenna resonance and to keep proper impedance matching.

3.2 | MIMO antenna design

For wideband performances, the proposed MIMO slot antennas are implemented symmetrically at the top and bottom sides of the ground plane, as illustrated in Figure 3. The

FIGURE 1 Configuration of the proposed slot antenna utilizing the bottom metal rim as GMT structuresAbbreviation: GMT, ground-mode tuning

FIGURE 2 Input impedance in a Smith chart: (A) with and without GMT, and (B) varied values of D in the slot antennaAbbreviation: GMT, ground-mode tuning

inductor pins at the top and bottom sides are $L1$ and $L2$ ($L1 = L2 = L = 8$ nH), respectively. In addition, the slot is exactly the same as that in Figure 1, except that the values of the lumped capacitor elements C in the slot are retuned as 0.84 pF. Two T-shaped decouplers are adopted, as shown in Figure 3, by connecting the left and right metal rims to the ground plane at the centers with inductor loads $L3$ and $L4$ ($L3 = 3.8$ nH, $L4 = 6$ nH), respectively. Therefore, the position of each inductor load can be simply assumed as the terminal location of each decoupler (port 4), and theoretical analysis of the
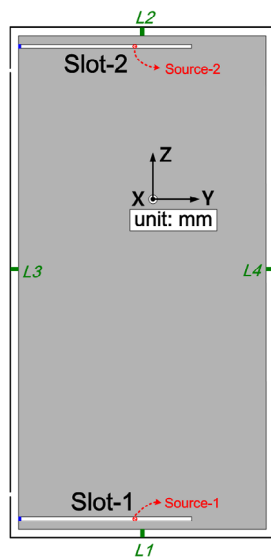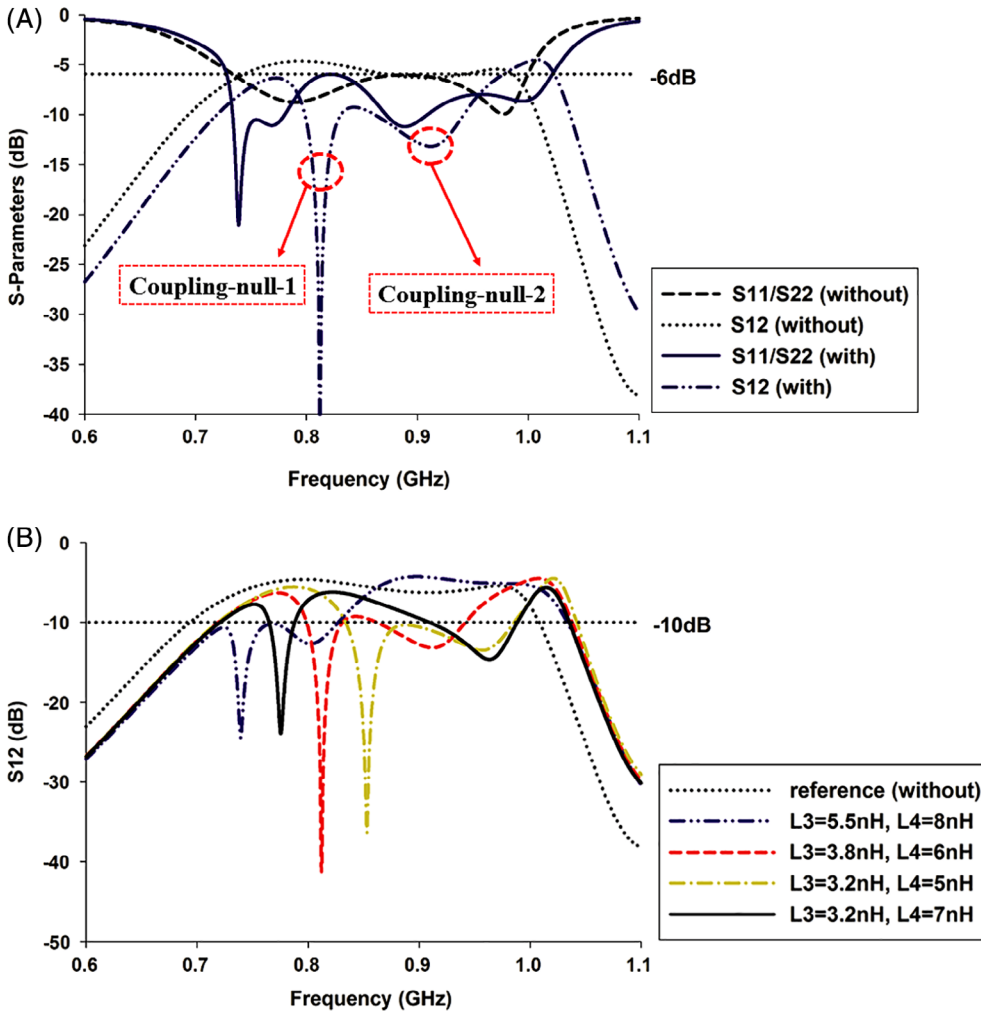

FIGURE 3 Configuration of the proposed MIMO antennas with two mode-based decouplersAbbreviation: MIMO, multiple-input multiple-output

decoupling theorem in Section 2 can be applied to each decoupler, independently and simultaneously.

Furthermore, the decouplers are designed in such a way that the mutual coupling between the decouplers and the ground mode along the length of the ground plane, *that is,* Z_{34}, is minimized to maintain high MIMO performance, according to the conditions of Equations (9)-(11). By referring to theoretical and experimental researches in the literature,[10–12,28,29] decouplers that are implemented at the electric field maximum of the dominant mode along the width of the ground plane (along y-axis) and the magnetic field maximum of the dominant mode along the length of the ground plane (along z-axis) operate as CCEs and can selectively excite the dominant ground mode y-axis, which is orthogonal to the dominant ground mode along z-axis, thereby guaranteeing minimal Z_{34}.

The scattering parameters with and without the proposed decouplers are shown in Figure 4A. The simulated reflection coefficients of both antennas with and without decouplers fully cover from 0.73 GHz to 1 GHz, and it can be seen that the decouplers do not degrade the bandwidth of the MIMO antennas, as can be expected according to Equations (9)-(11). A strong coupling (S_{12}) as high as -5 dB is generated between the two antennas without decouplers. Due to the decoupling effect, two coupling nulls are created in the S_{12} curve, and the isolation is significantly increased with a peak value of 40 dB, especially from 0.80 to 0.94 GHz. Note that the right-side decoupler generates the coupling null at the lower frequency (Coupling-null-1), while the left-side decoupler generates the one at the higher frequency (Coupling-null-2).

FIGURE 4 Simulated S-parameters of the proposed MIMO antennas: (A) S-parameters with and without decouplers, and (B) S_{12} variation by tuning decouplersAbbreviation: MIMO, multiple-input multiple-output

According to Equations (6) and (12), the loaded impedance (Z_L) at the decoupler should be optimized to achieve effective decoupling, which can be easily realized by lumped element. Furthermore, to avoid additional ohmic loss from the loaded element, only reactance component of Z_L is adopted. Generally, Z_L can be easily found in simulation by observing the variation of the S_{12} curve; consequently, the value of $L3$ and $L4$ can be tuned to provide a decoupling effect at a different frequency range, as can be seen from the S_{12} variations in Figure 4B. As $L3 = 5.5$ nH and $L4 = 8$ nH, the two nulls both shift to the lower frequency, providing isolation above 10 dB from 0.73 GHz to 0.83 GHz. When $L3 = 3.2$ nH and $L4 = 5$ nH, isolation above 10 dB with a peak value of 38 dB is generated, especially from 0.84 to 0.99 GHz. Similarly, the two nulls can be adjusted away from each other as $L3$ and $L4$ are tuned to 3.2 and 7 nH, respectively.

To better investigate the proposed mode-based decouplers, the simulated surface-current distributions of the proposed MIMO antennas in Figure 4A are presented in Figure 5. The data are generated when antenna 1 is excited and antenna 2 is loaded. At 0.8 GHz, which is within the frequency range of Coupling-null-1, the right-side decoupler operates dominantly, which can be seen from the dense current distributions at the right-side metal rim (see Figure 5A). Similarly, the left-side decoupler operates at 0.9 GHz (within Coupling-null-2). Moreover, less current is induced into the port of antenna 2 as well as the top-side metal rim, indicating the effectiveness of the proposed decoupling techniques. As can be seen from the current distributions over the metal rims in Figure 5 (red arrow lines), the two inductor-loaded decouplers are simultaneously operating at different resonant frequencies, providing high isolation in a wide bandwidth without degrading the antenna's radiation performance.

Simulated radiation patterns in *yz*-planes are demonstrated in Figure 6 to show the effect of the decouplers on the radiation-pattern modification. It can be observed that the E_θ components are dominant for both antennas. In addition, both antenna 1 and antenna 2 present radiation nulls with angle rotation in the E_θ components, providing diagonally directed dipole-type radiation patterns. At both 0.8 and 0.9 GHz, the diagonally directed radiation patterns of the two antennas are pointing away from each other with an approximately 60° angle difference, which is an important
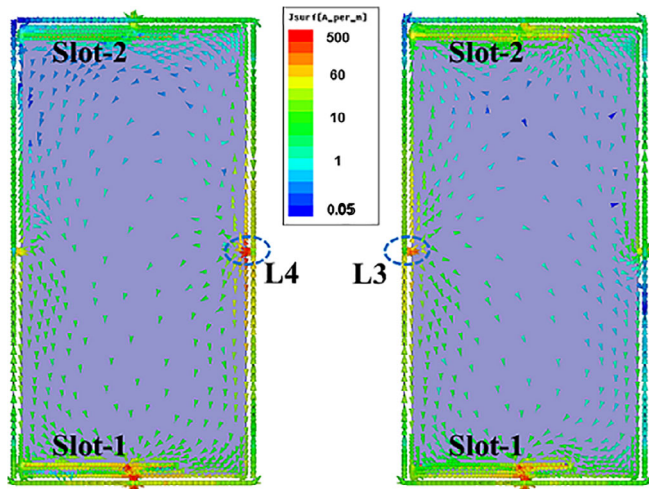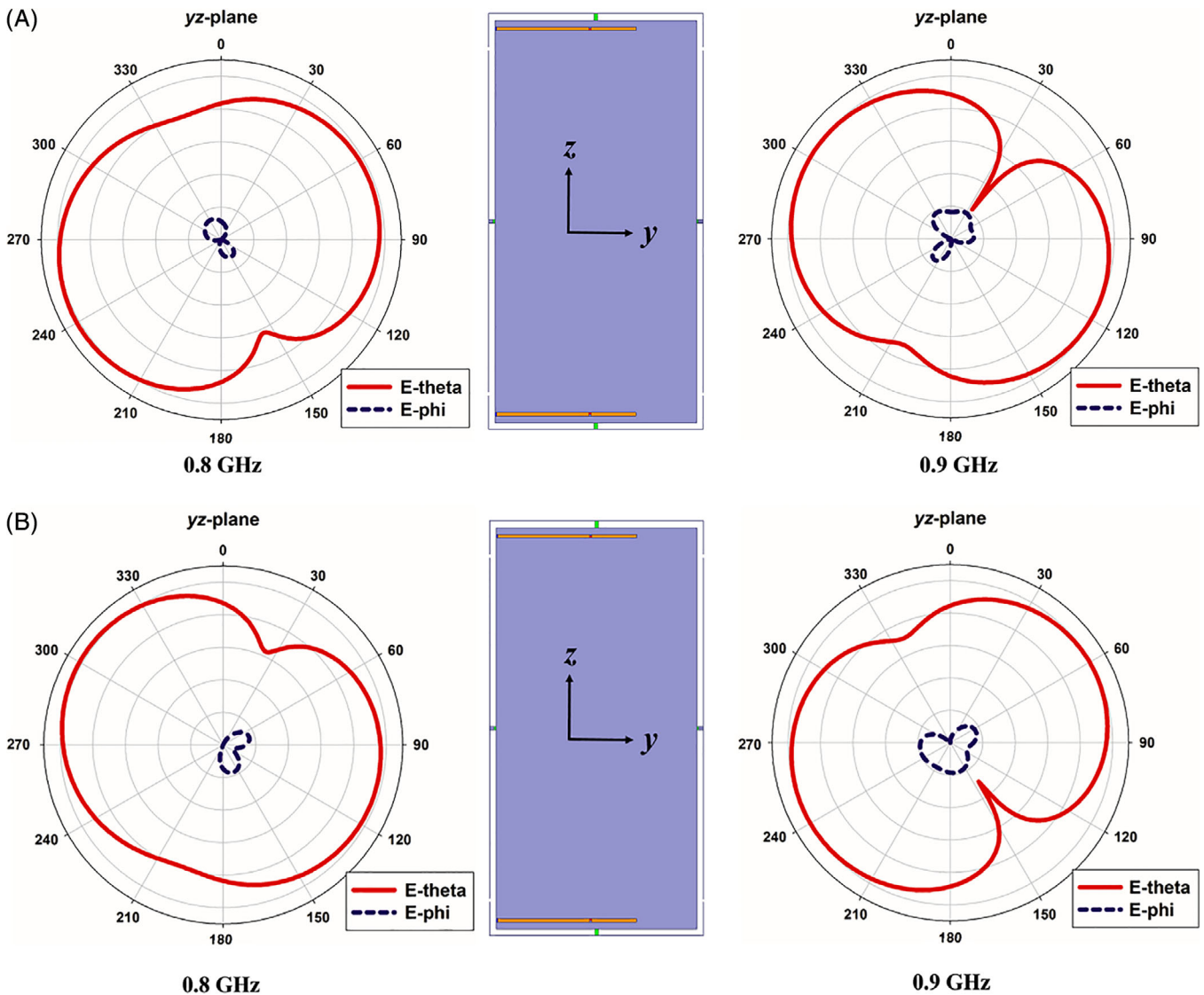
FIGURE 5 Simulated surface-current distributions with antenna 1 excitation: (A) at 0.8 GHz, and (B) at 0.9 GHz
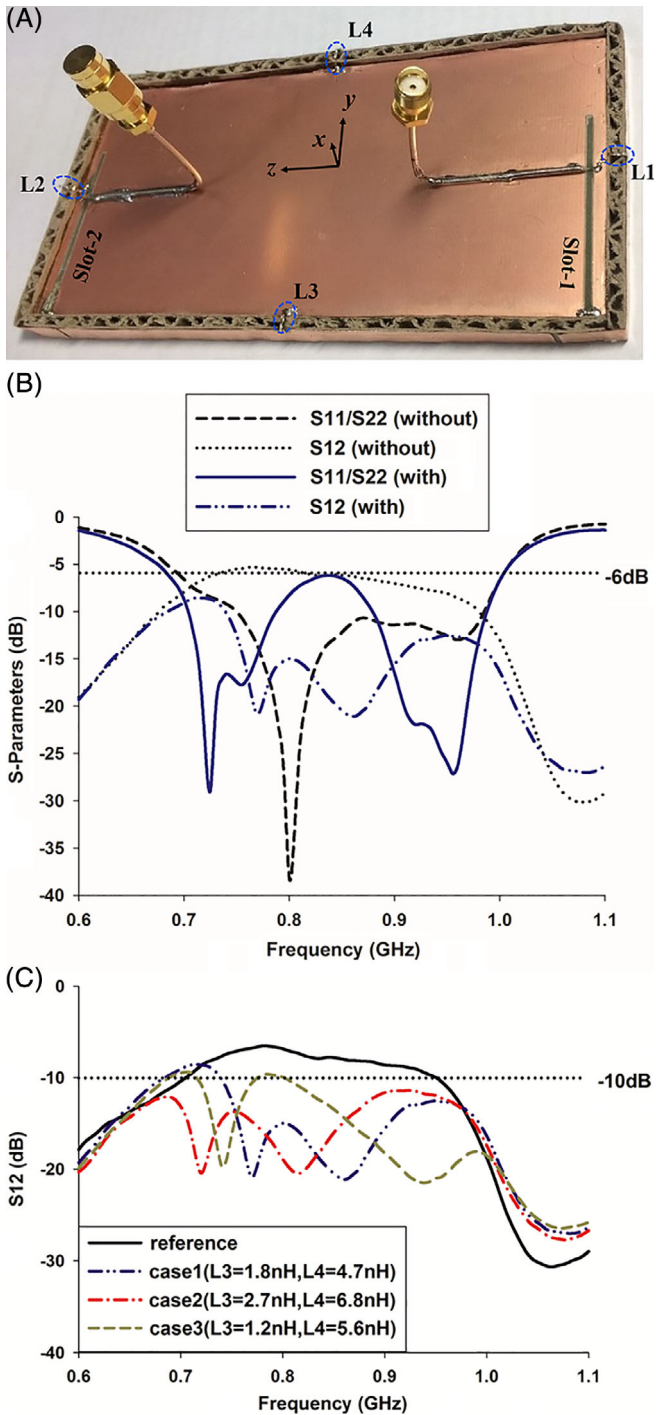
characteristic for diversity performance. The diagonally directed dipole-type radiation patterns can be seen as a combination of two orthogonal linear dipoles (z-directed and y-directed) that are in time phase or 180° out of phase. The radiation patterns can be explained by the current distributions of the decouplers in Figure 5, and both decouplers tightly couple to the dominant mode along the width of the ground plane (along the y-axis) at their operating frequencies.

3.3 | Measurement and discussion

To verify the proposed antenna designs, the proposed MIMO antennas were fabricated as shown in Figure 7A, and the scattering parameters with and without the decouplers are presented in Figure 7B. The measured S_{11}/S_{22} of the proposed MIMO antennas with decouplers fully cover from 0.69 to 1 GHz, and two coupling nulls in the S_{12} curve are
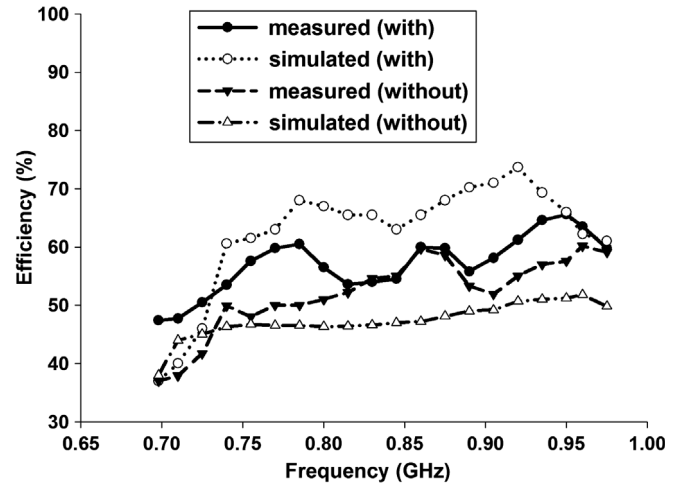

FIGURE 6 Simulated radiation patterns in yz-planes: (A) antenna 1 at 0.8 and 0.9 GHz, and (B) antenna 2 at 0.8 and 0.9 GHz

(A)

(B)

FIGURE 7 Measurement of the proposed MIMO antennas: (A) prototype of the fabricated antennas, (B) S-parameters of MIMO antennas with and without decouplers, and (C) S_{12} variation by tuning $L3$ and $L4$ Abbreviation: MIMO, multiple-input multiple-output

FIGURE 8 Total efficiencies of the proposed MIMO antennas for case 1 in simulation and measurement Abbreviation: MIMO, multiple-input multiple-output

simulated ones. Note that high-Q Murata 0402 LQG series chip inductors were used in the measurement, and the values for each case are shown in Figure 7C. In practice, a combination of inductors with various values can be simply chosen to satisfy different requirements.

The total efficiencies of the MIMO antennas with and without decouplers are conducted in both simulation and measurement by including the mismatching and the mutual coupling, as shown in Figure 8. Note that the simulated data are obtained in the case of Figure 4A, and the measured data are obtained in the case of Figure 7B. A 3D CTIA OTA anechoic chamber was used for measurement of the total efficiency including the reflection loss, where one port was measured with another port loaded with matched load. It can be observed that the total efficiencies are improved in both simulation and measurement by using the decouplers. The discrepancy between simulation and measurement can be attributed to the fabrication error and induced current into the semi-rigid cables. The simulated total efficiencies with decouplers are slightly higher than the measured ones, mainly due to extra loss from lumped elements and the semi-rigid cable. Whereas, the measured total efficiencies without decouplers are slightly higher than the simulated ones, and this is because both the reflection loss and mutual coupling loss are less severe in measurement resulted from the imperfect fabrication of the antenna structures. It is noted that the total measured efficiencies of the MIMO antennas with and without the proposed decouplers are approximately 60% and 50% on average, respectively. As a reference, the measured total efficiency of the single antenna is approximately 70%.

Furthermore, the radiation patterns of the proposed MIMO antennas for case 1 are measured and presented at 0.77 GHz, as plotted in Figure 9. It is noted that the right-side decoupler dominantly operates at 0.77 GHz in the

generated, providing high isolation from 9 dB to 20 dB. Note that the difference between simulation and measurement can be a result of extra loss in the fabrication. By varying the inductor values of $L3$ and $L4$ in the decouplers, the S_{12} curves are shown for three cases in Figure 7C, verifying the tunability and effectiveness of the proposed decouplers. Therefore, the measured results are consistent with the

measurement. As can be expected, the E_θ components are omnidirectional at the *xy*-plane, and the E_φ components are omnidirectional at the *xz*-plane. The *yz*-plane reveals that the maximum gains point away from each other, determining their diversity performance. Similar results with the simulated radiation patterns as diagonally directed dipole-type radiation patterns are observed.

Correlation is an important parameter for evaluating the diversity performance of the MIMO antennas, and it can be calculated in terms of the amplitude, phase, and polarization from the 3D far-field radiation patterns.[32] The envelope correlation coefficient (ECC) ρ_e can be simply used to measure the diversity performance, as

$$\rho_e = \frac{\left| \underset{4\pi}{\int \int} \left[\vec{F}_1(\theta,\varphi) \cdot \vec{F}_2(\theta,\varphi) \right] d\Omega \right|^2}{\underset{4\pi}{\int \int} \left| \vec{F}_1(\theta,\varphi) \right|^2 d\Omega \underset{4\pi}{\int \int} \left| \vec{F}_2(\theta,\varphi) \right|^2 d\Omega} \quad (13)$$

where $\vec{F}_i(\theta,\varphi)$ is the far-field radiation pattern of the antenna when port i is excited. Accordingly, the polarization diversity is utilized by the rotation of the current modes, which can be verified from the simulated and measured radiation patterns.
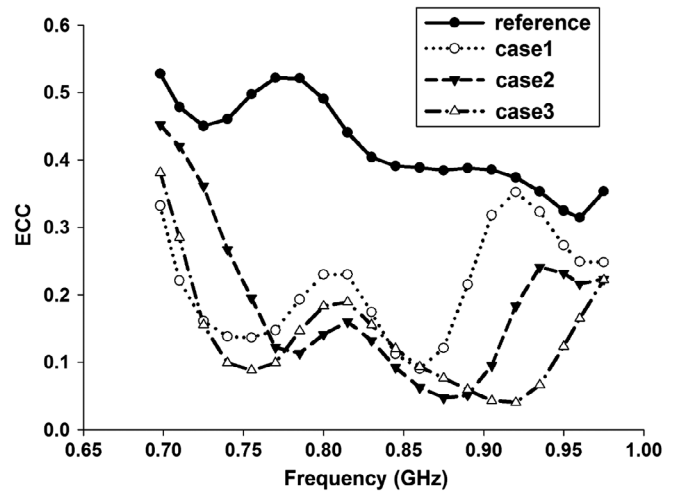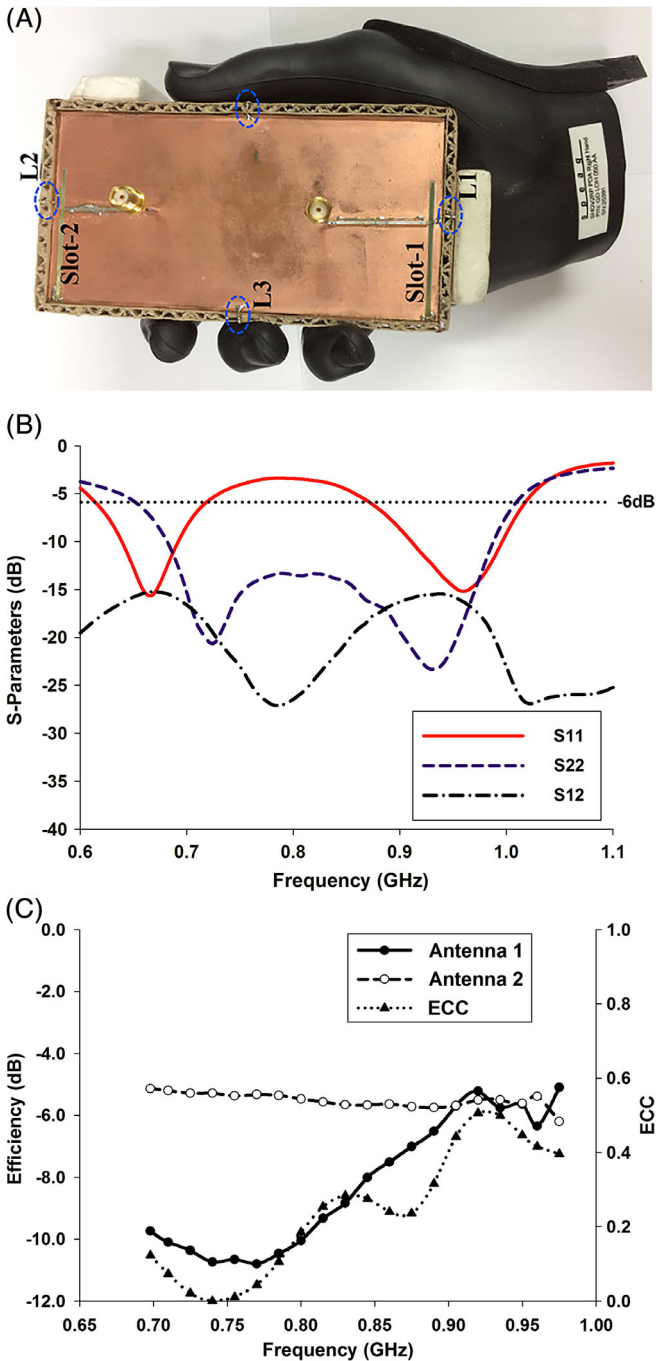

FIGURE 10 Measured ECC of the proposed MIMO antennasAbbreviations: ECC, envelope correlation coefficient; MIMO, multiple-input multiple-output

The figure-of-merit for satisfied diversity in mobile applications is $\rho_e < 0.5$.[32] Accordingly, the ECC values of the three cases in Figure 10 are plotted by measuring the 3D far-field radiation pattern (see Figure 9). The measured ECC of the MIMO antenna without decouplers ranges from 0.3 to 0.6, which is especially high at lower frequencies. The
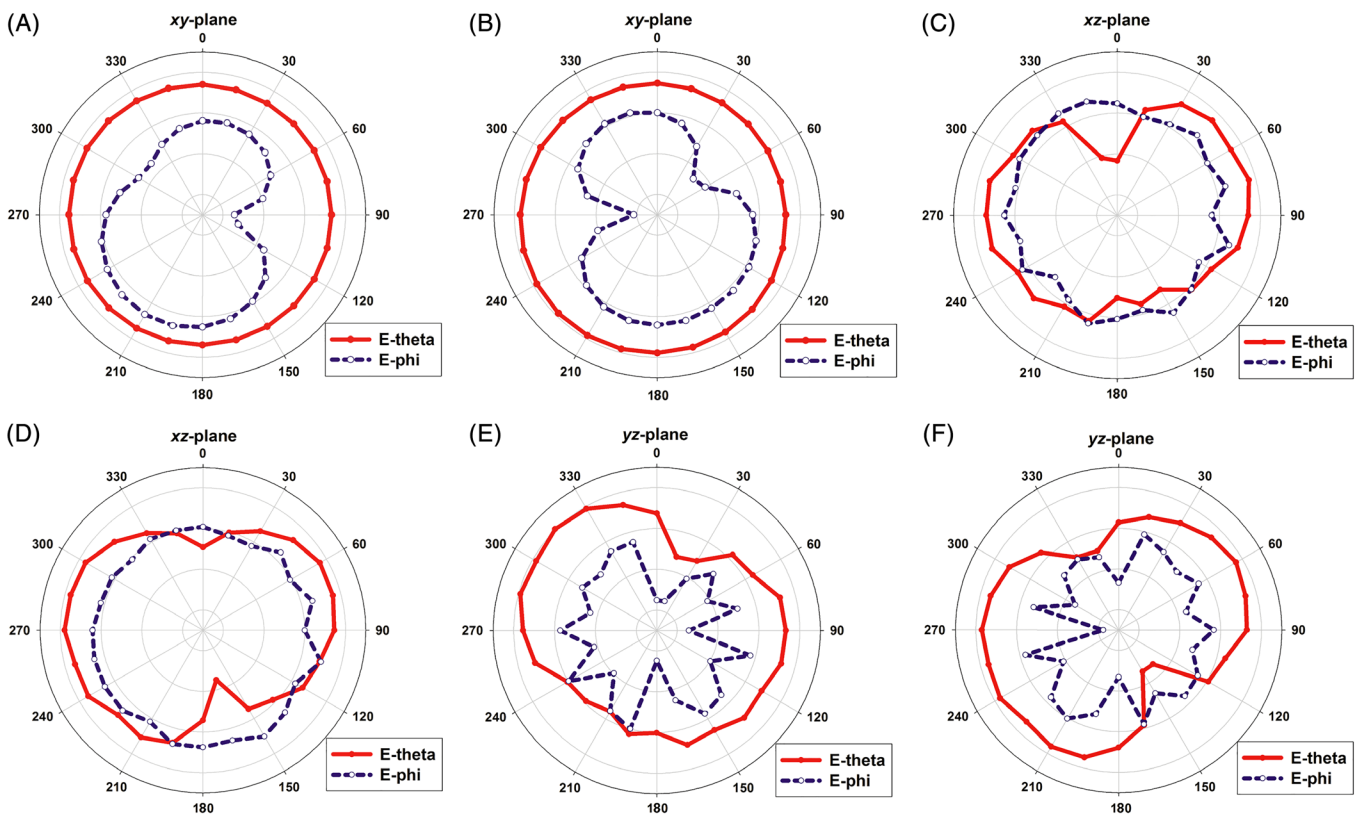
FIGURE 9 Measured radiation patterns at 0.77 GHz for the proposed MIMO antennas for case 1: (A) *xy*-plane for antenna 1, (B) *xy*-plane for antenna 2, (C) *xz*-plane for antenna 1, (D) *xz*-plane for antenna 2, (E) *yz*-plane for antenna 1, and (F) *yz*-plane for antenna 2Abbreviation: MIMO, multiple-input multiple-output

FIGURE 11 Measurement of the proposed MIMO antennas for case 1 with PDA right hand phantom: (A) PDA right hand phantom, (B) S-parameters, and (C) efficiencies and ECC valuesAbbreviations: ECC, envelope correlation coefficient; MIMO, multiple-input multiple-output; PDA, personal digital assistants

decouplers effectively decrease the ECC values, especially at the frequency range of the coupling nulls, providing ECC values from 0.05 to 0.4. Therefore, the proposed decoupling technique can simultaneously enhance the isolation and minimize the correlation within a wide bandwidth.

Furthermore, hand effect is of interest to observe in practice when the antennas are exposed to the users, so the antenna radiation performance as well as the diversity performance can be changed due to frequency shift, mismatching and power absorption.[33–35] The hand effect of the proposed MIMO antennas for case 1 (see Figure 7B) is investigated in Figure 11A, where a personal digital assistants (PDA) right hand phantom is used, and the position of the mobile device as well as the material properties of the phantom satisfy the measurement method of CTIA. Due to the hand effect, the S-parameters shown in Figure 11B are different from those in Figure 7B. It can be observed that the resonant frequency of antenna 1 shifts to the lower frequency, while that of antenna 2 is not greatly affected, which can be explained by the fact that the hand is closely touching the bottom metal rim but far away from the top metal rim. In the S_{12} curve, a wideband coupling null is generated due to the fingers loading in the right and left metal rims (decouplers). Furthermore, the coupling in the whole operating range is reduced, which can be expected from the reduced radiation performance. The total efficiencies and ECC values are measured to verify the radiation performance and the diversity performance of the proposed MIMO antennas, as shown in Figure 11C. As can be expected, antenna 1 has lower total efficiencies (averaging 20%) than antenna 2 (averaging 29%). Compared to those in free space (see Figure 8), approximately 5 dB and 3 dB reductions are generated for antenna 1 and antenna 2, respectively, which is in the acceptable range of 5~7 dB at the lower frequency and has comparable performance reported in References.[33–35] The ECC values are varied because of the shift of the coupling null and the variation of total efficiencies, generally providing lower values in lower frequencies and higher values in higher frequencies. Note that minor retuning is required to achieve a compromise between free space and hand application.

4 | CONCLUSION

This article demonstrated a comprehensive perspective on wideband small mobile-antenna design for both single and MIMO applications. Small slot antennas operating below 1 GHz were built utilizing the top and bottom metal rims for GMT, achieving wideband performance. Two novel mode-based decouplers utilizing the right and left metal rims were implemented by considering the ground-mode effect; thus, the proposed mode-based decouplers provided high isolation and diagonally directed radiation patterns without degrading the antenna performance. The measured results fully cover the low frequency band from 0.69 to 1 GHz, with high isolation (from 9 dB to 20 dB) and low ECC (from 0.05 to 0.4). Hand effects on the radiation performance and diversity performance are further investigated to verify the practicability of the proposed MIMO antennas. Therefore, the proposed small mobile antennas exhibited wideband, high isolation,

and low correlation performances through the proposed GMT and mode-based decoupling techniques.

ACKNOWLEDGMENT

ORCID

Longyue Qu https://orcid.org/0000-0001-5152-091X

REFERENCES

1. Sibille A, Oestges C, Zanella A. *MIMO: From Theory to Implementation*. San Diego, CA: Academic Press; 2011.

2. Wheeler HA. Fundamental limitations of small antennas. *Proc IRE*. 1947;35(12):1479-1484.

3. Zong W-H, Yang X-M, Li S, Qu X-Y, Wei X-Y. A compact slot antenna configuration for ultrawideband (UWB) terminals and mobile phones. *Int J RF Microw Comput Aided Eng*. 2018;28:e21400.

4. Wong K-L, Tsai C-Y. Half-loop frame antenna for the LTE metal-casing tablet device. *IEEE Trans Antennas Propag*. 2017;65(1):71-81.

5. Kang T-W, Wong K-L. Simple two-strip monopole with a parasitic shorted strip for internal eight-band LTE/WWAN laptop computer antenna. *Microw Opt Technol Lett*. 2011;53(4):706-712.

6. Lee J, Liu Y, Kim H. Mobile antenna using multi-resonance feed structure for wideband operation. *IEEE Trans Antennas Propag*. 2014;62(11):5851-5855.

7. Liu Y, Kim H-H, Kim H. Loop-type ground radiation antenna for dual-band WLAN applications. *IEEE Trans Antennas Propag*. 2013;61(9):4819-4823.

8. Qu L, Zhang R, Lee H, Kim H. Compact triple-band ground radiation antenna using two inner rectangular loops enclosed by two outer loops. *Electron Lett*. 2016;52(10):790-792.

9. Qu L, Zhang R, Kim H. Decoupling between ground radiation antennas with ground-coupled loop-type isolator for WLAN applications. *IET Microw Antennas Propag*. 2016;10(5):546-552.

10. Vainikainen P, Holopainen J, Kyro M. Antennas for digital television receivers in mobile terminals. *Proc IEEE*. 2012;100(7):2341-2348.

11. Lehtovuori A, Valkonen R, Ilvonen J. Designing capacitive coupling element antennas with bandwidth estimators. *IEEE Antennas Wireless Propag Lett*. 2014;13:959-962.

12. Vainikainen P, Ollikainen J, Kivekas O, Kelander K. Resonator-based analysis of the combination of mobile handset antenna and chassis. *IEEE Trans Antennas Propag*. 2002;50(10):1433-1444.

13. Qu L, Zhang R, Shin H, Kim J, Kim H. Mode-controlled wideband slot-fed ground radiation antenna utilizing metal loads for mobile applications. *IEEE Trans Antennas Propag*. 2017;65(2):867-872.

14. Schroeder WL, Famdie T, Solbach K. Utilisation and tuning of the chassis modes of a handheld terminal for the design. In Proc. IEE Wideband Multi-Band Antennas Arrays; Birmingham, UK; 2005:117-121.

15. Qu L, Zahid Z, Kim HH, Kim H. Circular polarized ground radiation antenna for mobile applications. *IEEE Trans Antennas Propag*. 2018;66(5):2655-2660.

16. Qu L, Jeon J, Park D, Kim H. Antenna design based on quasi-degenerate characteristic modes of unbroken metal rim. *IET Microw Antennas Propag*. 2017;11(15):2168-2173.

17. Li K, Shi Y. Wideband MIMO handset antenna design based on theory of characteristic modes. *Int J RF Microw Comput Aided Eng*. 2018;28:e21217.

18. Zou H, Li Y, Sim C-Y-D, Yang G. Design of 8×8 dual-band MIMO antenna array for 5G smartphone applications. *Int J RF Microw Comput Aided Eng*. 2018;28:e21420.

19. Chen Y, Manteuffel D. A tunable decoupling and matching concept for compact terminal antennas. *IEEE Trans Antennas Propag*. 2017;65(4):1570-1578.

20. Wang Y, Du Z. A wideband printed dual-antenna with three neutralization lines for mobile terminals. *IEEE Trans Antennas Propag*. 2014;62(3):1495-1500.

21. Chen A, Zhang J, Zhao L, Yin Y. A dual-feed MIMO antenna pair with one shared radiator and two isolated ports for fifth generation mobile communication band. *Int J RF Microw Comput Aided Eng*. 2017;27:e21146.

22. Lau BK, Andersen JB. Simple and efficient decoupling of compact arrays with parasitic scatters. *IEEE Trans Antennas Propag*. 2011;60(2):464-472.

23. See CH, Abd-Alhameed RA, McEwan NJ, Jones SMR, Asif R, Excell PS. Design of a printed MIMO/diversity monopole antenna for future generation handheld devices. *Int J RF Microw Comput Aided Eng*. 2015;25(6):510-521.

24. Chattha HT, Nasir M, Abbasi QH, Huang Y, AlJa'afreh SS. Compact low profile dual port single wideband planar inverted-F MIMO antenna. *Antenna Wirel Propag Lett*. 2013;12:1673-1675.

25. Pozar DM. *Microwave Engineering*. Hoboken, NJ: Wiley; 2005.

26. Huang L, Schroeder Werner L, Russer P. Estimation of maximum attainable antenna bandwidth in electrically small mobile terminals. In Proc. 36th Eur. Microw. Conf.; Manchester, UK; 2006:630-633.

27. Harrington RF, Mautz J. Theory of characteristic modes for conducting bodies. *IEEE Trans Antennas Propag*. 1971;19(5):622-628.

28. Martens R, Safin E, Manteuffel D. Selective excitation of characteristic modes on small terminals. In Proc. 5th Eur. Conf. Antennas Propag. (EuCAP); Rome, Italy; 2011:2492-2496.

29. Shih T-Y, Behdad N. Bandwidth enhancement of platform-mounted HF antennas using the characteristic mode theory. *IEEE Trans Antennas Propag*. 2016;64(7):2648-2659.

30. Baraniet IRR, Wong K-L. Dual-feed U-slot antenna having low envelope correlation coefficients for the LTE MIMO operation in the metal-framed smartphone. *Microw Opt Technol Lett*. 2018;60(2):295-302.

31. Wong K-L, Huang CY. Triple-wideband open-slot antenna for the LTE metal-framed tablet device. *IEEE Trans Antennas Propag*. 2015;63(12):5966-5971.

32. Vaughan RG, Andersen JB. Antenna diversity in mobile communications. *IEEE Trans Veh Technol*. 1987;36:149-172.

33. Zhang S, Zhao K, Ying Z, He S. Adaptive quad-element multi-wideband antenna array for user-effective LTE MIMO mobile terminals. *IEEE Trans Antennas Propag*. 2013;61(8):4275-4283.

34. Hsu C-K, Chung S-J. Compact multiband antenna for handsets with a conducting edge. *IEEE Trans Antennas Propag*. 2015;63(11):5102-5107.

35. Pelosi M, Franek O, Knudsen MB, Pedersen GF, Andersen JB. Antenna proximity effects for talk and data modes in mobile phones. *IEEE Antennas Propag Mag*. 2010;52(3):15-27.

AUTHOR BIOGRAPHIES
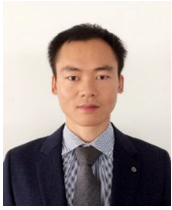
Longyue Qu received his BSc degree in communication engineering from the Yanbian University, China, in 2013, and the MSc and PhD degrees from the Hanyang University, Seoul, Rep. of Korea, in 2015 and 2018, respectively, in microwave engineering. He is currently a research fellow at Hanyang University. His current research interests include antenna theory and design especially for 4G/5G communications, massive MIMO, metamaterials, mmWave, and RF circuits. He serves as a reviewer for several international journals, such as IEEE Transactions on Antennas and Propagation, IEEE Antennas and Wireless Propagation Letters, IEEE Access.

Haiyan Piao received her BSc degree in communication engineering from the Yanbian University, China, in 2013. From 2013 to 2015, she served as an information technology researcher at China Telecom. She received the MSc degree in microwave engineering from the Hanyang University, Seoul, Rep. of Korea, in 2017. Her research interests are antenna design, MIMO, 5G communications, IoT, etc.

Hyeongdong Kim received his BS and MS degrees from Seoul National University, Rep. of Korea, in 1984 and 1986, respectively, and his PhD degree from the University of Texas, Austin, USA in 1992. From May 1992 to February 1993, he was a Post-Doctoral Fellow with the University of Texas. Since 1993, he has been a Professor with the Department of Electrical and Computer Engineering, Hanyang University, Rep. of Korea. His recent research interests include antenna theory and design especially for mobile devices, for example, wideband, high efficiency, multiband, MIMO, and high sensitivity.